GSA DATA REPOSITORY 2012259 **GAETANI ET AL.**

SUPPLEMENTAL MATERIAL

Definitions

(1) δD_{VSMOW} is the difference between the measured D/H ratio of a sample and the D/H ratio of Vienna Standard Mean Ocean Water (VSMOW) expressed in per mil (‰):

$$\delta D_{VSMOW} = 1000 \times \left[\frac{(D/H)_{Sample}}{(D/H)_{VSMOW}} - 1 \right] = 1000 \times \left[\frac{(D/H)_{Sample}}{0.00015576} - 1 \right].$$

(2) β is the exponent in Graham's law for diffusion of gases, which states that diffusivity is inversely proportional to the mass of the diffusing molecule. $\beta = 0.5$ for an ideal gas. Graham's law was used to estimate the relative diffusivities (D_i) of H^+ and D^+ from their relative masses (m) as follows:

$$\frac{D_{D^+}}{D_{H^+}} = \left(\frac{m_{H^+}}{m_{D^+}} \right)^{\beta}$$

Our experimental data suggest that $\beta \approx 0.2$ for diffusion of protons and deuterons in magnesian olivine.

Experimental Methods

Hydration experiments were conducted at 1250 °C and 1.0 GPa in pressure-sealed capsules fabricated from Ni metal (Ayers et al., 1992) using an end-loaded piston cylinder device (Boyd and England, 1960) and either a 1.27 cm (MID-1) or 1.91 cm (MID-2) diameter assembly. Inclusion-bearing olivine grains from Mauna Loa volcano were loaded into each capsule, along with isotopically labeled water ($D_2{}^{18}O$) and a Pt foil packet containing NiO to serve as an f_{O_2} buffer. Water was added, using a microsyringe, immediately before pressure sealing the capsule to minimize any potential evaporative loss. The capsule was centered in a straight-walled graphite furnace using crushable MgO spacers. The pressure medium for all experiments consisted of a CaF_2 sleeve. Pressure was applied using the cold piston-in technique (Johannes et al., 1971). The friction correction for the assemblies was calibrated against the Ca-Tschermakite breakdown reaction at 1.2 to 1.4 GPa and 1300 °C (Hays, 1966) and determined to be less than the pressure uncertainty associated with the experiments, so that no correction has been applied to the reported pressure. Temperature was measured and controlled using a $W_3Re_{97}/W_{25}Re_{75}$ thermocouple; no correction for the effect of pressure on thermocouple EMF has been applied to the reported temperature. Thermocouple oxidation over the course of an experiment was

minimized by flowing N_2 gas over the thermocouple wires. Temperatures are estimated to be accurate to ±10 °C and pressures to ±50 MPa, and the thermal gradient over the capsule was <5 °C. Experiments were terminated by shutting off the power. At the end of each experiment, a hole was drilled in the capsule to verify the presence of a free fluid phase. Experiment MID-1 remained buffered at Ni-NiO, but we were unable to verify the presence of nickel oxide in experiment MID-2 due to loss of the buffer packet, placing the maximum f_{O_2} at Ni-NiO.

Dehydration experiments were conducted at 1250 °C and 0.1 MPa in a Deltech vertical quenching furnace. Inclusion-bearing olivine grains from the 1999 eruption of Cerro Negro volcano were loaded into a Pt capsule that was crimped closed on both ends and suspended in the furnace hot spot. Temperature was continuously monitored using a Pt-$Pt_{90}Rh_{10}$ thermocouple and is estimated to be accurate to ±3 °C. The fugacity of oxygen was controlled near the Ni-NiO oxygen buffer using a CO_2–CO gas mixture, and monitored using a solid ZrO_2–CaO electrolyte oxygen sensor calibrated against the Fe–FeO and Ni–NiO buffers. Each experiment was terminated by dropping the Pt capsule into distilled H_2O.

Analytical Methods

Melt inclusion-bearing olivines recovered from the experiments were mounted in epoxy and polished to expose the inclusions. Olivines containing exposed inclusions were individually removed from the epoxy, using a temperature-controlled soldering iron, pressed into an In metal mount, to lower volatile blanks in the SIMS, and polished.

The major element compositions of melt inclusions and host olivines were determined using the 5-spectrometer JEOL 733 electron microprobe at the Massachusetts Institute of Technology. An accelerating voltage of 15 kV was used for all analyses. Olivine analyses were carried out using a beam diameter of 1 μm and a current of 30 nA. Counting times were 300 s for Fe and 40 s for all other elements. A beam current of 10 nA and beam diameter of 10-20 μm were used for all glass analyses. Counting times were 5 s for Na and 40 s for all other elements. Data were reduced using a modified ZAF procedure (Armstrong, 1988).

The water concentration, oxygen and hydrogen isotopic composition of experimental products were measured using the Cameca IMS 1280 ion microprobe in the Northeast National Ion Microprobe Facility at Woods Hole Oceanographic Institution. A beam of $^{133}Cs^+$ ions with a current of 1.6±0.1 nA was focused into a spot of ~ 15μm in diameter and was rastered over 30 x 30μm area. A mechanical aperture was placed at the secondary ion image plane such that effectively only the central 15 x 15μm area was analyzed. For hydration experimental products, secondary ion intensities of ^{18}O, ^{17}O, ^{16}OH, and ^{30}Si were measured with a mass resolving power of ~5500. The water concentration was determined in melt inclusions using $^{16}OH/^{30}Si$ ratios calibrated by analyses of glass standards of known water content. The $^{18}O/^{17}O$ was used to measure the uptake of ^{18}O into olivines and melt inclusions. Both melt inclusions and the interiors of olivine crystals were found to be indistinguishable from natural abundance values of basaltic glass and olivine, with $^{18}O/^{17}O$ = 5.19±0.02 and 5.22±0.18, respectively. The hydrogen

isotope ratios were measured by $^{16}OD/^{16}OH$ for both hydration and dehydration experimental products with a mass resolving power of ~8500 (Fig. A2). Secondary ion intensities of ^{16}OH, ^{16}OD, and ^{30}Si were measured in an ascending mass order and the cycle was repeated 50 times. For untreated melt inclusions from Cerro Negro with 3.8±0.3 wt% H_2O, $^{16}OD/^{16}OH$ ratios were determined with a precision of ±2‰ (1σ).

Samples were prepared for X-ray absorption near edge structure spectroscopy (XANES) by removing them from the In mounts and polishing the olivine to wafers ~40 μm thick, so that melt inclusions were doubly exposed and contamination by any signal from the olivine could be avoided. Iron K-edge XANES spectra were measured at beamline GSECARS 13-ID-C of the Advanced Photon Source at Argonne National Laboratory, using a micro-focused X-ray beam and a Si (111) monochromator. Spectra were recorded in fluorescence mode from 7,010 to 7,418 eV. A step sizes of 5 eV was used from 7,010 to 7,100 eV, 0.25 eV from 7,100 to 7,145 eV, and 5 eV above 7,145 eV. An Fe foil spectrum was used to calibrate the first-derivative peak of the Fe K-edge to be 7,112.0 eV. Centroid positions were determined by fitting the baseline with an arctangent, and the pre-edge peaks with two Lorentzians from 7107.5 to 7120.75 eV. Working curves relating $Fe^{3+}/\Sigma Fe$ to centroid energy were constructed using the basaltic standard glasses of Cottrell et al. (2009) (Fig. A3).

Melt Inclusion Dehydration Calculations

The calculations presented in Fig. 4 were carried out as follows. First, open system degassing paths were calculated, using VolatileCalc (Newman and Lowenstern, 2002), for two magmas – one containing 0.5 wt% H_2O and 2023 ppm CO_2, and a second with 6.5 wt% H_2O and 873 ppm CO_2 – as they decompress from 500 to 300 MPa. In each case it is assumed that the magma body is ascending from the mantle to a crustal magma reservoir slowly enough that the H_2O contents of melt inclusions formed at 500 MPa maintain equilibrium with the external magma. Second, changes to the internal pressure of melt inclusions due to H_2O loss at constant volume and constant temperature were calculated using MELTS (Asimow and Ghiorso, 1998; Ghiorso and Sack, 1995). Third, the effect on internal pressure of volume changes to the inclusion related to expansion of the host olivine during decompression were calculated using the Equation 21 of Zhang (1998) and elastic moduli compiled by Bass (1995). Finally, the concentration of CO_2 in each of the melts was calculated, using VolatileCalc, at the new pressure and H_2O content.

REFERENCES

Armstrong, J. T., 1988, Quantitative analysis of silicate and oxide minerals: comparison of Monte Carlo, ZAF, and ϕ(ρz) procedures, *in* Newbury, D. E., ed., Microbeam Analysis - 1988: San Francisco, CA, San Francisco Press, p. 239-246.

Asimow, P. D., and Ghiorso, M. S., 1998, Algorithmic modifications extending MELTS to calculate subsolidus phase relations: American Mineralogist, v. 83, p. 1127-1131.

Ayers, J. C., Brenan, J. B., Watson, E. B., Wark, D. A., and Minarik, W. G., 1992, A new capsule technique for hydrothermal experiments using the piston-cylinder apparatus: American Mineralogist, v. 77, no. 9-10, p. 1080-1086.

Bass, J. D., 1995, Elasticity of minerals, glasses and melts, *in* Ahrens, T. J., ed., Mineral physics and crystallography: a handbook of physical constants: Washington, DC, American Geophysical Union, p. 45-63.

Boyd, F. R., and England, J. L., 1960, Apparatus for phase equilibrium studies studies at pressures up to 50 kbar and temperatures up to 1750 °C: Journal of Geophysical Research, v. 65, p. 741-748.

Cottrell, E., Kelley, K. A., Lanzirotti, A., and Fischer, R., 2009, High-precision determination of iron oxidation state in silicate glasses using XANES: Chemical Geology, v. 268, p. 167-179.

Ghiorso, M. S., and Sack, R. O., 1995, Chemical mass transfer in magmatic processes IV. A revised and internally consistent thermodynamic model for the interpolation and extrapolation of liquid-solid equilibria in magmatic systems at elevated temperatures and pressures: Contributions to Mineralogy and Petrology, v. 119, p. 197-212.

Hays, J. F., 1966, Lime-alumina-silica: Carnegie Institution of Washington Yearbook, v. 65, p. 234-239.

Johannes, W., Bell, P., Mao, H. K., Boettcher, A. L., Chipman, D. W., Hays, J. F., Newton, R. C., and Seifert, F., 1971, An interlaboratory comparison of piston-cylinder pressure calibration using the albite-breakdown reaction: Contributions to Mineralogy and Petrology, v. 32, p. 24-38.

Kress, V. C., and Carmichael, I. S. E., 1991, The compressibility of silicate liquids containing Fe_2O_3 and the effect of composition, temperature, oxygen fugacity and pressure on their redox states: Contributions to Mineralogy and Petrology, v. 108, p. 82-92.

Newman, S., and Lowenstern, J. B., 2002, VolatileCalc: a silicate melt-H_2O-CO_2 solution model written in Visual Basic for excel: Computers and Geoscience, v. 28, p. 597-604.

Ryerson, F. J., Durham, W. B., Cherniak, D. J., and Lanford, W. A., 1989, Oxygen diffusion in olivine: effect of oxygen fugacity and implications for creep: Journal of Geophysical Research, v. 94, no. B4, p. 4105-4118.

Zhang, Y., 1998, Mechanical and phase equilibria in inclusion-host systems: Earth and Planetary Science Letters, v. 157, p. 209-222.

Table DR1. Summary of starting materials, experimental conditions, and results.

Experiment	Duration (h)	$log\ f_{O_2}^{Expt}$	H_2O (wt%)	δD_{VSMOW}	$^{18}O/^{17}O$	$Fe^{3+}/\Sigma Fe$	ΔNiNiO
Mauna Loa melt inclusions							
K97-17-1	—	—	0.398(5)	—	5.23(9)	0.212(15)	+0.1(2)
K97-17-2a	—	—	0.373(5)	—	5.22(11)	0.230(12)	+0.35(16)
K97-17-2b	—	—	0.360(5)	—	—	0.222(5)	+0.25(6)
K97-17-3	—	—	0.373(5)	—	—	0.246(14)	+0.56(17)
K97-17-4	—	—	0.372(5)	—	—	0.223(14)	+0.25(18)
Hydration experiments							
MID-1	22	-7.01	3.90(5)	—	5.19(9)	0.192(6)	-0.04(8)
MID-2a	48	-7.01	1.69(2)	—	5.20(6)	0.164(13)	-0.6(2)
MID-2b	48	-7.01	3.75(5)	—	5.2(2)	—	—
Cerro Negro melt inclusions							
CN1	—	—	2.74(4)	25(4)	—	—	—
CN2	—	—	4.89(7)	-2.4(3)	—	0.55(3)	+3.8(2)
CN3	—	—	4.11(6)	11(2)	—	0.532(12)	+3.58(11)
CN4	—	—	3.46(5)	23(3)	—	0.571(15)	+4.01(14)
CN5	—	—	4.11(6)	37(5)	—	0.640(16)	+4.58(16)
CN6	—	—	3.76(5)	2.2(3)	—	0.600(18)	+4.26(17)
Dehydration experiments							
CN99DH4-2	1	-7.00	1.70(2)	170(30)	—	0.271(6)	+1.50(7)
CN99DH4-3	1	-7.00	1.70(2)	66(10)	—	0.497(4)	+4.07(4)
CN99DH4-4	1	-7.00	2.84(4)	35(5)	—	0.352(6)	+2.13(6)
CN99DH4-5	1	-7.00	2.62(4)	45(7)	—	—	—
CN99DH2-2	3	-7.08	2.31(3)	110(16)	—	0.306(6)	+1.71(6)
CN99DH2-3	3	-7.08	2.44(3)	74(11)	—	—	—
CN99DH2-6	3	-7.08	0.136(2)	390(60)	—	—	—
CN99DH1-1	18	-6.96	0.064(1)	-35(5)	—	0.223(3)	+0.64(4)
CN99DH1-4	18	-6.96	0.093(1)	380(60)	—	—	—
CN99DH1-5	18	-6.96	0.058(1)	140(20)	—	—	—
CN99DH1-6	18	-6.96	0.098(1)	450(70)	—	0.232(3)	+0.76(4)

Notes: ΔNiNiO is the oxygen fugacity corresponding to the measured $Fe^{3+}/\Sigma Fe$ ratio, calculated using the model of Kress and Carmichael (1991), expressed relative to the Ni-NiO oxygen buffer. Units in parentheses represent 1σ uncertainties in terms of least unit cited calculated by propagating standard errors based on replicate analysis. Therefore 0.398(5) should be read as 0.398 ± 0.005.

Table DR2. Summary of SIMS analyses of olivines from hydration experiments.

Distance from edge of olivine (μm)	H_2O (ppm)	$^{18}O/^{17}O$
Experiment MID-1		
21	101.0(19)	5.10(17)
84	86.2(16)	5.6(11)
143	73.6(14)	5.6(10)
Experiment MID-2		
246	74.3(14)	5.2(2)
287	62.8(12)	5.10(14)
338	70.0(13)	5.18(16)
387	85.0(16)	5.13(11)
489	73.3(14)	5.12(8)
527	82.5(15)	5.23(15)
583	82.3(15)	5.16(7)
641	69.4(13)	5.15(7)
722	50.0(9)	5.14(6)

Notes: Units in parentheses are the same as on Table DR1.

Table DR3. Electron microprobe analyses of melt inclusions and host olivines

Sample	Phase	n	SiO_2	TiO_2	Al_2O_3	FeO*	MnO	MgO	CaO	Na_2O	K_2O	P_2O_5	S	Total
Mauna Loa melt inclusions														
K97-17-1	Gl	3	52.61(9)	2.14(2)	13.50(4)	9.23(8)	0.14(1)	8.39(4)	10.73(4)	2.13(2)	0.37(1)	0.22(2)	0.014(6)	99.47
	Oliv	10	40.00(12)	—	—	11.90(6)	0.12(1)	47.61(7)	0.20(1)	—	—	—	—	99.83
K97-17-2a	Gl	3	52.49(6)	1.99(2)	13.56(8)	8.93(1)	0.14(1)	8.33(5)	10.43(12)	2.45(9)	0.51(1)	0.23(6)	0.172(7)	99.23
	Oliv	10	40.36(11)	—	—	11.4(3)	0.12(1)	48.0(3)	0.21(1)	—	—	—	—	100.09
K97-17-2b	Gl	3	52.79(13)	2.01(6)	13.61(4)	8.77(10)	0.13(2)	8.16(4)	10.49(8)	2.39(10)	0.49(2)	0.21(2)	0.157(10)	99.21
	Oliv	10	40.26(7)	—	—	11.8(3)	0.12(1)	47.6(3)	0.22(3)	—	—	—	—	100.00
K97-17-3	Gl	3	52.91(8)	2.04(7)	13.53(6)	8.78(1)	0.12(1)	8.30(2)	10.34(3)	2.37(7)	0.44(2)	0.21(3)	0.138(8)	99.18
	Oliv	10	40.13(7)	—	—	11.8(3)	0.11(1)	47.9(2)	0.21(2)	—	—	—	—	100.15
K97-17-4	Gl	3	52.43(10)	1.97(2)	13.55(8)	9.08(9)	0.14(1)	8.14(7)	10.80(4)	2.33(7)	0.45(1)	0.23(5)	0.132(17)	99.25
	Oliv	10	39.97(8)	—	—	12.3(3)	0.12(2)	47.5(3)	0.24(2)	—	—	—	—	100.13
Hydration experiments														
MID-1	Gl	3	49.39(4)	1.56(6)	11.65(8)	8.50(5)	0.14(1)	11.16(14)	8.99(5)	2.01(10)	0.34(1)	0.20(2)	0.060(5)	94.00
	Oliv	10	40.08(8)	—	—	11.76(9)	0.15(1)	48.41(15)	0.19(1)	—	—	—	—	100.59
MID-2a	Gl	2	55.1(3)	1.81(6)	13.47(8)	6.18(4)	0.14(1)	3.6(6)	10.4(3)	2.08(4)	0.35(4)	0.29(1)	0.085(1)	93.51
MID-2b	Gl	3	48.9(3)	1.84(4)	13.25(6)	8.43(16)	0.13(2)	9.87(4)	10.17(9)	2.38(5)	0.42(2)	0.20(2)	0.069(7)	95.66
	Oliv	10	40.2(2)	—	—	11.9(3)	0.16(1)	47.7(6)	0.20(1)	—	—	—	—	100.16
Cerro Negro melt inclusions														
CN1	Gl	3	49.0(6)	1.09(5)	14.73(11)	13.67(5)	0.24(1)	5.60(6)	8.7(2)	1.6(10)	0.56(4)	0.14(2)	0.061(7)	95.39
	Oliv	10	38.09(8)	—	—	25.06(16)	0.43(2)	38.07(11)	0.18(2)	—	—	—	—	101.83
CN2	Gl	3	42.98(13)	1.38(4)	17.44(2)	10.56(7)	0.20(1)	7.51(3)	11.68(7)	1.44(8)	0.20(1)	0.13(1)	0.046(8)	93.57
	Oliv	10	38.95(07)	—	—	17.94(12)	0.30(1)	43.6(2)	0.20(1)	—	—	—	—	100.99
CN3	Gl	3	44.23(19)	1.41(4)	16.92(10)	10.50(5)	0.20(1)	7.23(4)	10.87(11)	1.94(13)	0.31(1)	0.19(2)	0.105(7)	93.91
	Oliv	10	38.94(15)	—	—	19.2(5)	0.28(1)	42.6(3)	0.19(2)	—	—	—	—	101.21
CN4	Gl	3	48.4(2)	1.06(1)	15.05(15)	12.89(11)	0.26(2)	5.61(10)	8.69(7)	2.57(13)	0.57(2)	0.16(2)	0.083(11)	95.34
	Oliv	10	38.1(5)	—	—	24.7(2)	0.44(1)	38.0(5)	0.16(1)	—	—	—	—	101.40
CN5	Gl	3	44.71(6)	0.68(3)	17.31(11)	10.43(11)	0.19(1)	7.00(9)	11.60(3)	1.60(7)	0.25(2)	0.09(1)	0.127(4)	93.99
	Oliv	10	38.75(7)	—	—	18.97(8)	0.29(1)	42.5(3)	0.18(1)	—	—	—	—	100.69
CN6	Gl	3	45.97(18)	0.75(2)	16.11(5)	11.42(3)	0.19(1)	6.70(6)	10.52(16)	1.64(8)	0.29(2)	0.09(1)	0.117(3)	93.80
	Oliv	10	38.44(15)	—	—	20.6(2)	0.32(2)	41.4(2)	0.17(1)	—	—	—	—	100.93

Table DR3. Continued.

Sample	Phase	n	SiO_2	TiO_2	Al_2O_3	FeO*	MnO	MgO	CaO	Na_2O	K_2O	P_2O_5	S	Total
Dehydration experiments														
CN99DH4-2	Gl	3	41.6(5)	0.60(1)	12.32(9)	20.6(3)	0.35(1)	11.2(5)	8.24(13)	1.66(4)	0.24(1)	0.09(1)	0.105(8)	97.00
	Oliv	10	38.53(11)	—	—	21.71(8)	0.35(1)	40.81(16)	0.18(1)	—	—	—	—	101.58
CN99DH4-3	Gl	2	37.26(15)	2.77(4)	12.44(1)	25.0(3)	0.36(1)	11.72(11)	6.39(6)	1.04(3)	0.30(1)	0.13(2)	0.115(5)	97.53
CN99DH4-4	Gl	3	43.1(5)	0.29(1)	13.9(3)	12.70(19)	0.19(1)	14.1(4)	9.5(2)	1.16(2)	0.11(1)	0.04(1)	0.054(9)	95.14
	Oliv	10	39.36(10)	—	—	17.30(8)	0.28(1)	44.40(15)	0.19(1)	—	—	—	—	101.53
CN99DH4-5	Gl	3	43.7(3)	0.50(1)	13.2(3)	17.02(3)	0.24(5)	11.9(4)	8.94(2)	1.48(6)	0.16(1)	0.10(1)	0.099(6)	97.34
	Oliv	10	38.94(9)	—	—	19.79(7)	0.29(2)	42.5(2)	0.18(1)	—	—	—	—	101.70
CN99DH2-2	Gl	3	43.2(4)	0.48(3)	13.22(12)	15.2(2)	0.24(1)	13.41(13)	8.78(6)	1.51(4)	0.22(1)	0.07(1)	0.110(9)	96.44
CN99DH2-3	Gl	3	44.91(17)	0.64(3)	13.09(3)	13.5(2)	0.21(1)	13.54(9)	8.47(4)	1.85(11)	0.33(2)	0.10(4)	0.073(3)	96.71
CN99DH2-6	Gl	3	43.3(4)	0.74(1)	13.01(10)	21.03(15)	0.33(1)	10.0(2)	8.01(18)	2.06(1)	0.44(2)	0.28(3)	0.219(5)	99.42
CN99DH1-1	Gl	3	41.58(18)	0.66(4)	15.92(7)	16.99(5)	0.25(2)	10.55(9)	11.33(5)	1.81(6)	0.25(1)	0.10(2)	0.135(15)	99.58
CN99DH1-4	Gl	3	42.7(3)	0.52(1)	14.67(15)	15.9(4)	0.24(2)	10.54(9)	12.13(7)	1.73(4)	0.17(1)	0.14(2)	0.112(13)	98.85
CN99DH1-5	Gl	3	42.0(3)	0.68(1)	16.00(17)	16.57(13)	0.26(2)	10.48(7)	10.6(3)	1.97(7)	0.26(1)	0.11(2)	0.133(9)	99.06
CN99DH1-6	Gl	3	43.31(17)	0.66(2)	15.78(11)	15.92(9)	0.26(1)	10.54(13)	10.2(4)	2.04(4)	0.37(1)	0.13(1)	0.128(3)	99.34
	Oliv	10	39.25(9)	—	—	17.26(5)	0.26(1)	44.46(10)	0.17(1)	—	—	—	—	101.40

Notes: Compositions are reported in weight percent. Abbreviations are as follows: Gl=glass, Oliv=olivine, n = number of analyses included in reported mean. Units in parentheses represent 1σ uncertainties on the basis of replicate analyses in terms of least unit cited. Therefore 52.61(9) should be read as 52.61 ± 0.09.

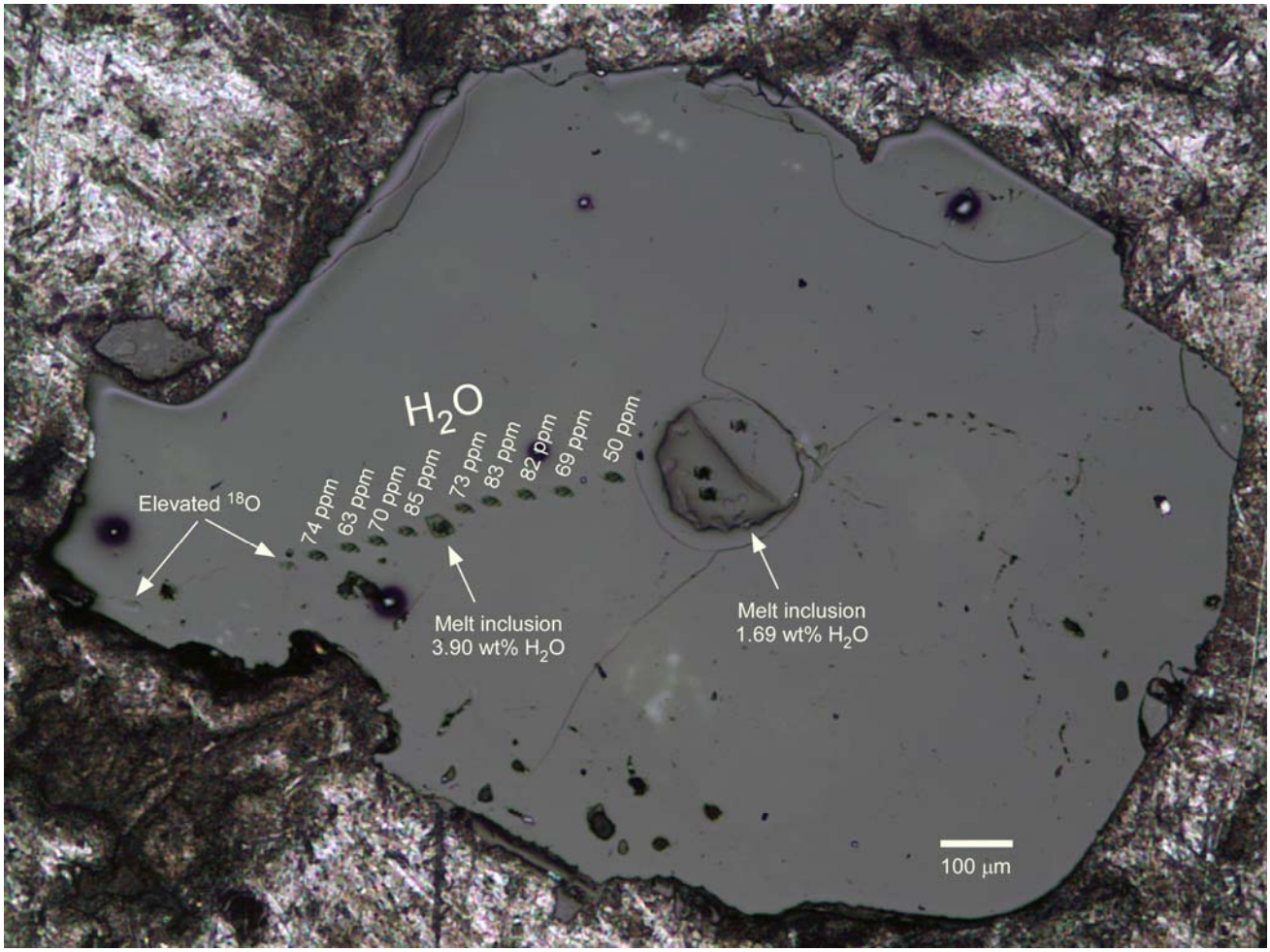

Figure DR1. Reflected light photomicrograph of an olivine, containing two melt inclusions, that was equilibrated with $D_2{}^{18}O$ at 1250 ºC and 1.0 GPa, for 48 hours. The melt inclusions have different water contents: the small inclusion close to edge of the grain has 3.90±0.05 wt% while the large inclusion in the center contains 1.69±0.02 wt% and has $Fe^{3+}/\Sigma Fe = 0.160\pm0.018$. The $^{18}O/^{17}O$ ratios of melt inclusions (5.19±0.08) and the interior of olivine crystal (5.15±0.04) are indistinguishable from one another. There is no systematic variation in $^{18}O/^{17}O$ ratio with distance from the edge of the grain, consistent with slow diffusion of O^{2-} in olivine (Ryerson et al., 1989). Elevated $^{18}O/^{17}O$ ratios are confined to the re-crystallized outer portions of the olivine grain, and are too high to quantify because ^{18}O count rates exceed the limit for the electron multiplier (2.5×10^6 counts/s).

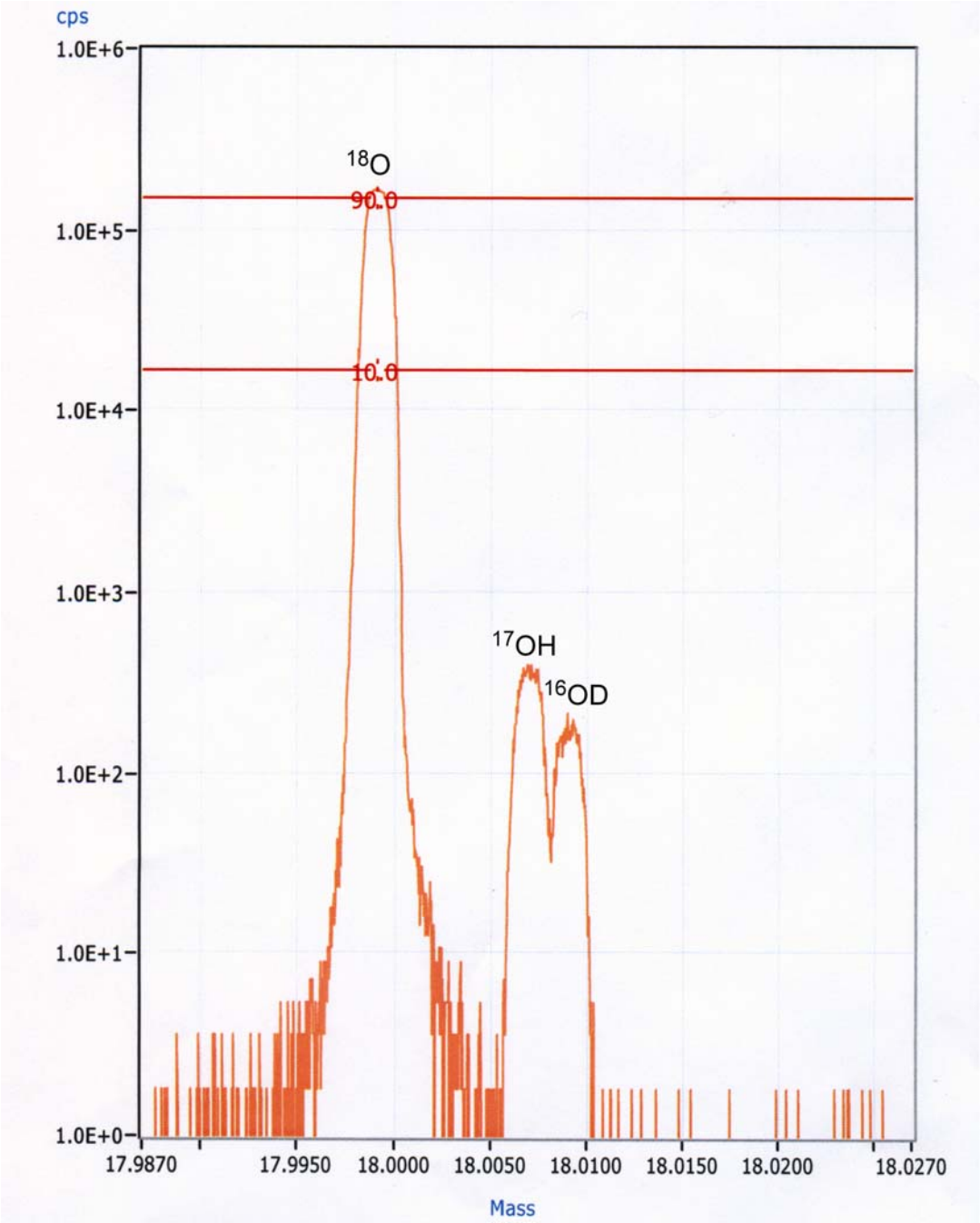

Figure DR2. A mass spectrum from the Cameca IMS 1280 ion microprobe in the Northeast National Ion Microprobe Facility at Woods Hole Oceanographic Institution over the mass region 17.99-18.03 for basaltic glass containing 1.5 wt% H_2O. For melt inclusions hydrated with D_2O, ions ^{16}OH, ^{17}O, ^{16}OH, ^{18}O, ^{16}OD, and ^{30}Si were measured. At a mass resolving power of 8900, masses ^{18}O, ^{17}OH, and ^{16}OD are clearly resolved. For dehydration experiments, only masses ^{16}OH, ^{16}OD, and ^{30}Si were measured. D/H ratios were corrected for instrumental mass fractionation by repeat analyses of D30, a basaltic glass sample of known hydrogen isotopic composition. The precision of repeat analyses of D30 was ± 12 ‰, 2σ, n = 6.

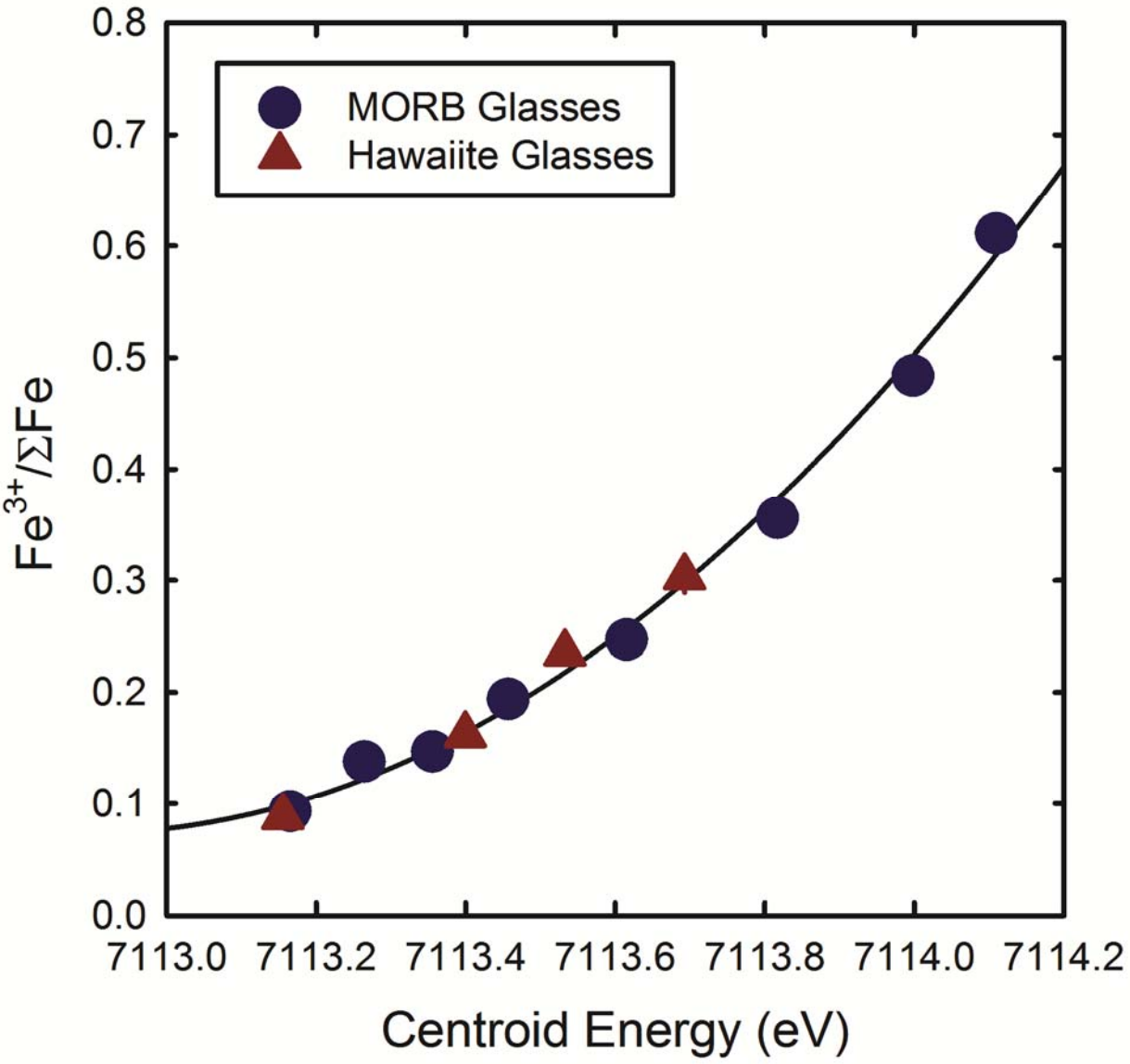

Figure DR3. Centroid energy versus $Fe^{3+}/\Sigma Fe$ determined at beamline GSECARS 13-ID-C of the Advanced Photon Source at Argonne National Laboratory for 12 basaltic glasses equilibrated experimentally over a broad range of fo_2 by Cottrell et al. (2009). A second-order polynomial fit to these data was used to convert centroid energy to $Fe^{3+}/\Sigma Fe$ for the melt inclusions in this study.